International Journal of Structural Stability and Dynamics

https://doi.org/10.1142/S021945542250016X

Flutter Analysis of a 3-D Box-Wing Aircraft Configuration

Amirhossein Ghasemikaram[*,§], Abbas Mazidi[*,¶,‖], S. Ahmad Fazelzadeh[†] and Dieter Scholz[‡]

[*]*Department of Mechanical Engineering*
School of Engineering, Yazd University
Safaiyeh, P.O. Box 89195-741, Yazd, Iran

[†]*Department of Mechanical Engineering*
School of Engineering, Shiraz University
Molla Sadra Ave., P.O. Box 71345, Shiraz, Iran

[‡]*Department of Aeronautical and Automotive Engineering*
University of Applied Sciences (HAW Hamburg)
Berliner Tor 9 20099, Hamburg, Germany
[§] *Ah.ghasemi@stu.yazd.ac.ir*

[†] [¶] *Amazidi@yazd.ac.ir*
Fazelzad@shirazu.ac.ir
[‡] *Info@profscholz.de*

The aim of the current paper is to present a flutter analysis of a 3-D Box-Wing Aircraft (BWA) configuration. The box wing structure is considered as consisting of two wings (front and rear wings) connected with a winglet. Plunge and pitch motions are considered for each wing and the winglet is modeled by a longitudinal spring. In order to exert the effect of the wing-joint interactions (bending and torsion coupling), two ends of the spring are located on the gravity centers of the wings tip sections. Wagner unsteady model is used to simulate the aerodynamic force and moment on the wing. The governing equations are extracted via Hamilton's variational principle. To transform the resulting partial integro-differential governing equations into a set of ordinary differential equations, the assumed modes method is utilized. In order to confirm the aerodynamic model, the flutter results of a clean wing are compared and validated with the previously published results. Also, for the validation, the 3-D box wing aircraft configuration flutter results are compared with MSC NASTRAN software and good agreement is observed. The effects of design parameters such as the winglet tension stiffness, the wing sweep and dihedral angles, and the aircraft altitude on the flutter velocity and frequency are investigated. The results reveal that physical and geometrical properties of the front and rear wings and also the winglet design have a significant influence on BWA aeroelastic stability boundary.

‖ Corresponding author.

1. Introduction

Box Wing Aircraft (BWA) is one of innovative configurations commonly used by airplane designers to reduce the aircraft emissions. Initial investigations on the box wings were implemented by Prandtl [1] who introduced the box wing aircraft as the best wing system that dramatically decreases the induced drag. A reduction of induced drag in the BWA has significant influence on the airplane weight and performance. Moreover, the reduction of induced drag has other benefits such as reduction of geometric dimensions and fuel consumption. On the other hand, the reduction of the wing span, due to using front and rear wings, could decrease the traffic problems at airports for midsize and large airplanes such as Boeing 747, Airbus 380 and Antonov 225.

Due to the great importance of the box wings, many researches have been conducted in the field of design and consequently, various types of configurations have been introduced to the international scientific society such as diamond wings, struts- and truss-braced wings, box-wing and PrandtlPlane configurations. Wolkovitch, [2] Livne and Weisshaar, [3, 4] and Cavallaro and Demasi [5] comprehensively reviewed the previous efforts on the joined-wing configurations, and accurately expressed the challenges, ideas and innovations on the configurations. In a Master of Science thesis at Pisa University, the basic design of a 250 passenger PrandtlPlane aircraft (PrP250) was investigated.[6] Torenbeek et al.[7] have discussed the important challenges of European Union such as the quality of aircraft wings, environmental issues, flight safety and air fleet performance in this work. In addition, he compared the induced drag between an optimal box wing and conventional wing. Frediani et al.[8] presented the methodologies used to design a class of PrandtlPlane ULM aircraft. The methodologies met the design requirements such as high visibility, low noise in cabin, and low stall speeds and enhanced the safety. Jansen and Perez [9] inquired the multidisciplinary design and optimization of non-planar configurations. They considered the coupling between aerodynamic and structure for different aircraft sizes and mission requirements. The results revealed the performance effects on the design of the configurations. Barcala et al. [10] stated that the existence of the front and rear wings in different planes can make the aerodynamic analysis of box wing configurations by theoretical/computational methods even more difficult. Therefore, they analyzed an experimental investigation on several configurations of the box wings. In the research project “IDINTOS” at Pisa University, Frediani et al.[11] designed and manufactured an ultralight amphibious PrandtlPlane prototype and some of the benefit results were figured out by means of both numerical and experimental analyses. There are also some other efforts in the field of joined-wing design which have evaluated the design requirements of the different configurations such as aerodynamics, flight mechanics, and weight optimization.[12-16]

Although numerous studies have been conducted on wing aeroelasticity, [17-25] a preliminary literature review shows that most previous studies on box wings are focused on design and aerodynamic performance. Lange et al. [26] studied the design of a transonic

box wing and remarked that "because of the complexity of the configuration, proper assessment of airplane characteristics utilizing this concept can only be accomplished by the use of rather elaborate analytical procedures for aerodynamic, structural loading and aeroelastic characteristics". Moreover, the existence of two wings separated in different planes has made the BWA aeroelastic analysis by theoretical or computational methods a difficult task. Hence, the vast majority of researchers have recently investigated the BWA aeroelastic analysis via professional software, [27-32] and a limited progress has been made on the mathematical modeling of aeroelastic BWA configurations.

Regarding the nonlinear aeroelasticity of the joined-wing configurations, in the recent years a number of studies have been published employing a discrete time-domain state-space approach which can convert the nonlinear system to a set of sub-linear systems. Each sub-linear system is considered to be linear whose response can be computed by a straight forward time integration. These studies are focused on the nonlinear systems due to large deformations (Chao et al. [33]), geometric nonlinearities (Blair et al., [34]) and nonlinear aerodynamic effects (Cavallaro et al. [35] and Alizadeh et al. [36]).

In the linear aeroelastic analysis, flutter speed and frequency are obtained with a smaller value compared to nonlinear cases. If the wing aspect ratio is low, the linear analysis can be accurate. On the other hand, because of the simplicity of solving the linear governing equations, many researchers prefer to utilize the linear aeroelastic analysis. Mirabbashi et al. [37] analyzed the flutter of an airfoil carrying a flexibly mounted unbalanced engine by analytical and experimental approaches. The typical wing section and the connected engine are modeled by a 5DOF system. The results revealed that some parameters of the engine can decrease the flutter boundary e.g. mass, pylon length and thrust. Ajaj et al. [38] studied the flutter of a telescopic, multi-segment and span morphing wing. They considered the wing as a stepped and cantilever Euler-Bernoulli beam and showed that the span morphing can augment the flutter boundary.

Durham and Ricketts [39] concluded that the particular joined-wing configuration can have higher flutter velocity in the high altitude compared to high aspect ratio configurations and they could prove their claim using wind tunnel tests. Van Aken [40] perused the feasibility of using active controls to postpone the whirl-flutter on a joined-wing configuration. He utilized the CAMRAD/JA code to extract the governing equations (a set of linear differential equations). The flutter analysis showed that the active control can delay the onset of tilt-rotor whirl-flutter. Lee [41] developed a methodology for aeroelastic design of the joined-wing configuration. The stability boundaries were obtained using Rayleigh-Ritz and finite element methods and the effective parameters on the aeroelastic behavior were also assessed. The results illustrated that the body-freedom flutter velocities decrease as fuselage flexibility increases. Furthermore, the center of gravity location and pitch moment of inertia can affect flutter boundary. Canto et al. [42] expressed the PrandtlPlane aircraft as a new concept for European air fleet in 2020. They discussed the design parameters such as maximum stress, ailerons performance, static aeroelasticity and flutter for optimization of the structural weight. Divoux and Frediani [43] studied the flutter characteristics of a lifting

system of a PrandtlPlane. They determined the flutter boundary of PrP250 using MSC NASTRAN software. Two different strategies were adopted to increase the flutter boundary; these include increased skin thickness and addition of tip tanks. The results showed that adding 20% thickness to the front wing and 10% to the rear wing, changes the flutter speed to the maximum value. Some new findings on the aeroelasticity of bow wings and PrandtlPlane configurations (a subgroup of joined-wings) are presented by Bombardieri et al.[44, 45] Their work shows two contributions: the first case is a critical literature review of the efforts tackling aeroelasticity of box wings and the second contribution is concerned with the aeroelastic analysis considering the antisymmetric modes. Furthermore, they have described the parameters affecting the flutter of box wings such as the location of fuel-tank, rigid-body modes, freeplay of control surfaces, and the front wing tip's region. Silvani and Cavallaro et al. [46, 47] investigated the aeroelastic behavior of the PrP250 aircraft. The flutter analysis revealed when composite materials are used in the PrandtlPlane structure, the flutter issues are completely overcome. Recently, Fazelzadeh et al. [48] solved the aeroelastic governing equations of the typical wing section of BWA configuration. They considered plunge and pitch motions for each wing section and modeled the torsion and bending elasticity using two torsional and longitudinal springs; also, the winglet was modeled by a longitudinal spring. The flutter analysis showed that the connection winglet stiffness and angle have significant effect on the box wing flutter speed and frequency. Due to the great importance of the aeroelastic static and dynamic phenomena on the joined-wing configurations, recently, CORIDS (Community Research and Development Information Service) and INEA (Innovation and Networks Executive Agency) have published public information on PARSIFAL project.[49]

Therefore, there is not yet a wide literature studying the aeroelasticity of box wings and several aspects need to be understood and analyzed in more depth. In the present study, aeroelastic modeling and flutter analysis of a 3-D box wing aircraft configuration are carried out. The results of this study can help designers to introduce small modifications to the design or come up with new BWA configurations that would avoid the flutter problem.

2. Governing Equations

A schematic of a BWA configuration is presented in Fig. 1. Because of the geometrical and dynamic complexity of the BWA, several intermediate coordinate systems are applied in this paper. The coordinate system $X_0Y_0Z_0$ and $(XYZ)_{f,r}$ are fixed on the air plane center of gravity and the root of each wing, respectively. Also the coordinate systems *xyz* and *x′y′z′* are located on the root of each un-deformed swept wing and the deformed swept wing, respectively.

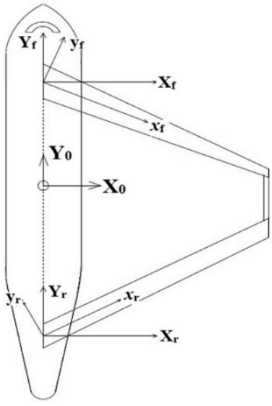

(a)

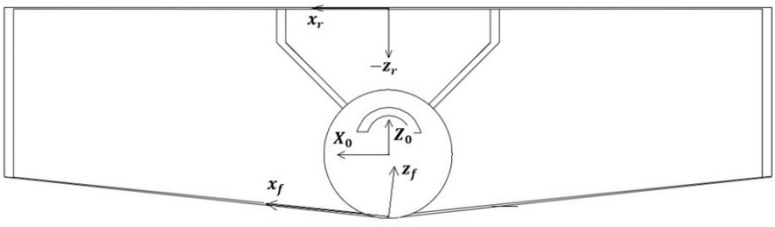

(b)

Fig. 1. A schematic of the BWA intermediate coordinate systems (a) Top view (b) Front view

The transformation between (xyz) f and (xyz) r coordinate systems is as described by Ref. (17). The subscripts f and r denote front and rear wings, respectively.

$$\hat{i}_r = [\cos\Gamma_f \cos(\Lambda_f + \Lambda_r)]\hat{i}_f + [\sin(\Lambda_f + \Lambda_r)]\hat{j}_f - [\sin\Gamma_f \cos(\Lambda_f + \Lambda_r)]\hat{k}_f$$

$$\hat{j}_r = -[\cos\Gamma_f \sin(\Lambda_f + \Lambda_r)]\hat{i}_f + \cos(\Lambda_f + \Lambda_r)\hat{j}_f + [\sin\Gamma_f \sin(\Lambda_f + \Lambda_r)]\hat{k}_f$$

$$\hat{k}_r = (\sin\Gamma_f)\hat{i}_f + (\cos\Gamma_f)\hat{k}_f \quad (1)$$

The box wing tip is shown in Fig. 2. The system consists of two bending and torsion deflections for the front wing (wf, θf) in zf and xf directions as well as two bending and torsion deflections for the rear wing (wr, θr) in zr and xr directions. It should be noted that in this paper, the winglet is modeled by a longitudinal spring and in order to consider the effect of the bending and torsion coupling, two ends of the spring are placed on the gravity centers of the wing sections.

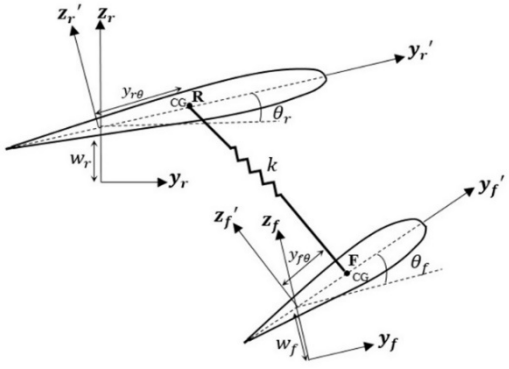

Fig. 2. Box wing tip by considering the winglet as a linear spring

It should be mentioned that *R* and *F* indexes indicate the center of gravity of the tip section of the rear and front wing before the deformation. A transformation between $(xyz)_{f,r}$ and $(x'y'z')_{f,r}$ coordinate systems is as described by Ref. (19).

$$\begin{aligned}
\hat{i}'_{f,r} &= \hat{i}_{f,r} + w'_{f,r}\,\hat{k}_{f,r} \\
\hat{j}'_{f,r} &= -w'_{f,r}\sin\theta_{f,r}\,\hat{i}_{f,r} + \cos\theta_{f,r}\,\hat{j}_{f,r} + \sin\theta_{f,r}\,\hat{k}_{f,r} \\
\hat{k}'_{f,r} &= -w'_{f,r}\cos\theta_{f,r}\,\hat{i}_{f,r} - \sin\theta_{f,r}\,\hat{j}_{f,r} + \cos\theta_{f,r}\,\hat{k}_{f,r}
\end{aligned} \tag{2}$$

The governing equations of motion are derived via Hamilton's variational principle that can be expressed as Ref. (20).

$$\int_{t_1}^{t_2}\left(-\delta T_t + \delta U_t + \delta U_k - \delta W_{n.c}\right)dt = 0 \tag{3}$$

$$\begin{aligned}
\vec{R}_f &= R_{yf}\hat{J}_f - R_{zf}\hat{K}_f + x_{1f}\hat{i}_f + y_{1f}\hat{j}_f + z_{1f}\hat{k}_f \\
&= \left[-R_{yf}\cos\Gamma_f\sin\Lambda_f + R_{zf}\sin\Gamma_f + x_f - \eta_f w'_f\sin\theta_f - \zeta_f w'_f\cos\theta_f\right]\hat{i}_f \\
&\quad + \left[R_{yf}\cos\Lambda_f + \eta_f\cos\theta_f - \zeta_f\sin\theta_f\right]\hat{j}_f \\
&\quad + \left[-R_{yf}\sin\Gamma_f\sin\Lambda_f - R_{zf}\cos\Gamma_f + w_f + \eta_f\sin\theta_f + \zeta_f\cos\theta_f\right]\hat{k}_f
\end{aligned} \tag{4}$$

$$\begin{aligned}
\vec{R}_r &= -R_{yr}\hat{J}_r + R_{zr}\hat{K}_r + x_{1r}\hat{i}_r + y_{1r}\hat{j}_r + z_{1r}\hat{k}_r \\
&= \left[-R_{yr}\sin\Lambda_f + x_r - \eta_r w'_r\sin\theta_r - \zeta_r w'_r\cos\theta_r\right]\hat{i}_r \\
&\quad + \left[-R_{yr}\cos\Lambda_r + \eta_r\cos\theta_r - \zeta_r\sin\theta_r\right]\hat{j}_r + \left[R_{zf} + w_r + \eta_r\sin\theta_r + \zeta_r\cos\theta_r\right]\hat{k}_r
\end{aligned} \tag{5}$$

where R_y and R_z indicate the distance between the center of gravity of the fuselage and the root of wings in y and z directions, respectively. x_1, y_1 and z_1 are the distances of an arbitrary point of the deformed wings from the root. So, the variation of kinetic energy for the left and right wings can be expressed as:

$$\delta T_f = -\int_0^{l_f} \iint_{A_f} m_f \ddot{\vec{R}}_f \bullet \delta \vec{R}_f \, d\zeta_f \, d\eta_f \, dx_f$$

$$= \left[\left(-m_f \ddot{w}_f + I_{\eta f} \ddot{w}_f'' - m_f y_{\theta f} \ddot{\theta}_f \right) \delta w_f + \left(-I_f \ddot{\theta}_f - m_f y_{\theta f} \ddot{w}_f \right) \delta \theta_f \right] dx_f \tag{6}$$

$$\delta T_r = -\int_0^{l_r} \iint_{A_r} m_r \ddot{\vec{R}}_r \bullet \delta \vec{R}_r \, d\zeta_r \, d\eta_r \, dx_r$$

$$= \left[\left(-m_r \ddot{w}_r + I_{\eta r} \ddot{w}_r'' - m_r y_{\theta r} \ddot{\theta}_r \right) \delta w_r + \left(-I_r \ddot{\theta}_r - m_r y_{\theta r} \ddot{w}_r \right) \delta \theta_r \right] dx_r \tag{7}$$

Also, the variation of the strain energy for the left and right wings is as the following equation.

$$\delta U_f = \int_0^{l_f} \left[E_f I_f w_f^{(4)} \delta w_f - G_f J_f \theta_f'' \delta \theta_f \right] dx_f \tag{8}$$

$$\delta U_r = \int_0^{l_f} \left[E_r I_r w_r^{(4)} \delta w_r - G_r J_r \theta_r'' \delta \theta_r \right] dx_r \tag{9}$$

where, *EI* and *GJ* are bending and torsional rigidity, respectively. To calculate the variation of the spring potential energy, the spring length before ($\Delta \mathbf{r}_1$) and after ($\Delta \mathbf{r}_2$) the deformation should be obtained as

$$\Delta \vec{r}_1 = \left[R_{yf} \hat{J}_f - R_{zf} \hat{K}_f + l_f \hat{i}_f + y_{\theta f} \hat{j}_f \right] - \left[-R_{yr} \hat{J}_r + R_{zr} \hat{K}_r + l_r \hat{i}_r + y_{\theta r} \hat{j}_r \right] \tag{10}$$

$$\Delta \vec{r}_2 = \left[R_{yf} \hat{J}_f - R_{zf} \hat{K}_f + l_f \hat{i}_f + w_f \delta_D \left(x_f - l_f \right) \hat{k}_f + y_{\theta f} \hat{j}_f' \right]$$
$$- \left[-R_{yr} \hat{J}_r + R_{zr} \hat{K}_r + l_r \hat{i}_r + w_r \delta_D \left(x_r - l_r \right) \hat{k}_r + y_{\theta r} \hat{j}_r \right] \tag{11}$$

The vector of spring deformation and the variation of spring potential energy can be expressed as Eqs. (12) and (13), respectively.

$$\Delta \vec{r} = \Delta \vec{r}_1 - \Delta \vec{r}_2 \tag{12}$$

$$\delta U_k = \int_0^{l_f} \int_0^{l_r} \left[k \, \Delta \vec{r} \bullet \delta \Delta \vec{r} \right] \delta_D \left(x_f - l_f \right) \delta_D \left(x_r - l_r \right) dx_r \, dx_f \tag{13}$$

The variational virtual work of the aerodynamic forces and moments acting on the box wing can be expressed according to the following relations.

$$\delta W_{nc,f} = \int_0^{l_f} \left[-L_f \, \delta w_f + M_f \, \delta \theta_f \right] dx_f \tag{14}$$

$$\delta W_{n.c.,r} = \int_0^{l_r} \left[-L_r \, \delta w_r + M_r \, \delta \theta_r \right] dx_r \tag{15}$$

where L and M refer to the aerodynamic lift and moment, respectively. By substituting Eqs. (6-9) and Eqs. (13-15) into the Hamilton's variational principle, the PIDEs are derived as Eqs. (16-19). Note that for every admissible variation (δw_f, $\delta\theta_f$, δw_r, $\delta\theta_r$), the coefficient of these variations must be zero.

$$\begin{aligned} & m_f \ddot{w}_f - I_{\eta f} \ddot{w}_f'' + m_f y_{\theta f} \ddot{\theta}_f + E_f I_f w_f^{(4)} + \int_0^{l_r} \{ k w_f \left[\delta_D \left(x_f - l_f \right) \right]^3 \delta_D \left(x_r - l_r \right) \\ & + k y_{\theta f} \theta_f \left[\delta_D \left(x_f - l_f \right) \right]^3 \delta_D \left(x_r - l_r \right) - k a_{33} w_r \left[\delta_D \left(x_f - l_f \right) \right]^2 \left[\delta_D \left(x_r - l_r \right) \right]^2 \\ & - k a_{33} y_{\theta r} \theta_r \left[\delta_D \left(x_f - l_f \right) \right]^2 \left[\delta_D \left(x_r - l_r \right) \right]^2 \} dx_r + L_f = 0 \end{aligned} \tag{16}$$

$$\begin{aligned} & I_f \ddot{\theta}_f + m_f y_{\theta f} \ddot{w}_f - G_f J_f \theta_f'' + \int_0^{l_r} \{ k y_{\theta f} w_f \left[\delta_D \left(x_f - l_f \right) \right]^3 \delta_D \left(x_r - l_r \right) \\ & + k y_{\theta f}{}^2 \theta_f \left[\delta_D \left(x_f - l_f \right) \right]^3 \delta_D \left(x_r - l_r \right) - k a_{33} y_{\theta f} w_r \left[\delta_D \left(x_f - l_f \right) \right]^2 . \left[\delta_D \left(x_r - l_r \right) \right]^2 \\ & - k a_{33} y_{\theta f} y_{\theta r} \theta_r \left[\delta_D \left(x_f - l_f \right) \right]^2 \left[\delta_D \left(x_r - l_r \right) \right]^2 \} dx_r - M_f = 0 \end{aligned} \tag{17}$$

$$\begin{aligned} & m_r \ddot{w}_r - I_{\eta r} \ddot{w}_r'' + m_r y_{\theta r} \ddot{\theta} + E_r I_r w_r^{(4)} + \int_0^{l_f} \{ k a_{31}{}^2 w_r \left[\delta_D \left(x_f - l_f \right) \right]^3 . \delta_D \left(x_r - l_r \right) \\ & + k a_{31}{}^2 y_{\theta r} \theta_r \left[\delta_D \left(x_f - l_f \right) \right]^3 \delta_D \left(x_r - l_r \right) + k a_{32}{}^2 w_r \left[\delta_D \left(x_f - l_f \right) \right]^3 \delta_D \left(x_r - l_r \right) \\ & + k a_{32}{}^2 y_{\theta r} \theta_r \left[\delta_D \left(x_f - l_f \right) \right]^3 . \delta_D \left(x_r - l_r \right) - k a_{33} w_f \left[\delta_D \left(x_f - l_f \right) \right]^2 \left[\delta_D \left(x_r - l_r \right) \right]^2 \\ & - k a_{33} y_{\theta f} \theta_f \left[\delta_D \left(x_f - l_f \right) \right]^2 \left[\delta_D \left(x_r - l_r \right) \right]^2 + k a_{33}{}^2 w_r \left[\delta_D \left(x_f - l_f \right) \right]^3 \delta_D \left(x_r - l_r \right) \\ & + k a_{33}{}^2 y_{\theta r} \theta_r \left[\delta_D \left(x_f - l_f \right) \right]^3 \delta_D \left(x_r - l_r \right) \} dx_f + L_r = 0 \end{aligned} \tag{18}$$

$$\begin{aligned} & I_r \ddot{\theta}_r + m_r y_{\theta r} \ddot{w}_r - G_r J_r \theta_r'' + \int_0^{l_f} \{ k a_{31}{}^2 y_{\theta r} w_r \left[\delta_D \left(x_f - l_f \right) \right]^3 . \delta_D \left(x_r - l_r \right) \\ & + k a_{31}{}^2 y_{\theta r}{}^2 \theta_r \left[\delta_D \left(x_f - l_f \right) \right]^3 \delta_D \left(x_r - l_r \right) + k a_{32}{}^2 y_{\theta r} w_r \left[\delta_D \left(x_f - l_f \right) \right]^3 \\ & \times \delta_D \left(x_r - l_r \right) + k a_{32}{}^2 y_{\theta r}{}^2 \theta_r . \left[\delta_D \left(x_f - l_f \right) \right]^3 \delta_D \left(x_r - l_r \right) - k a_{33} y_{\theta r} w_f \\ & \times \left[\delta_D \left(x_f - l_f \right) \right]^2 . \left[\delta_D \left(x_r - l_r \right) \right]^2 - k a_{33} y_{\theta f} y_{\theta r} \theta_f \left[\delta_D \left(x_f - l_f \right) \right]^2 . \left[\delta_D \left(x_r - l_r \right) \right]^2 \\ & + k a_{33}{}^2 y_{\theta r} w_r \times \left[\delta_D \left(x_f - l_f \right) \right]^3 \delta_D \left(x_r - l_r \right) + k a_{33}{}^2 y_{\theta r}{}^2 \theta_r . \left[\delta_D \left(x_f - l_f \right) \right]^3 \\ & \times \delta_D \left(x_r - l_r \right) \} dx_f - M_r = 0 \end{aligned} \tag{19}$$

3. Wagner Unsteady Model

In order to employ the aerodynamic loadings, Wagner unsteady model is utilized.[24, 25] Because of the wing sweep angle, some corrections should be implemented in the aerodynamic model. The following procedure is utilized by Ref. (21, 23).

$$\dot{w}_{f,r} + U\theta_{f,r} \rightarrow \dot{w}_{f,r} + U\cos\Lambda_{f,r}\theta_{f,r} + U\sin\Lambda_{f,r}w'_{f,r} \tag{20}$$

$$\dot{\theta}_{f,r} \rightarrow \dot{\theta}_{f,r} + U\sin\Lambda_{f,r}\theta'_{f,r} \tag{21}$$

For the finite-span wings, the modified Strip theory is used to extend 2-D model to 3-D case. Therefore, the following corrections should be applied to the aerodynamic lift and moment.

$$C_{l\theta} = \frac{dC_l}{d\theta} = \frac{2\pi.AR}{AR\sqrt{1+\left(\frac{2\cos\Lambda}{AR}\right)^2} + 2\cos\Lambda} \tag{22}$$

$$\frac{1}{2}b = \frac{b}{2}\left(\frac{C_{l\theta}}{\pi} - 1\right) \tag{23}$$

where *A.R.* and $C_{l\theta}$ are the wing aspect ratio and the lift-curve slope, respectively. The final relations can be expressed after applying the corrections as follows:

$$\begin{aligned}
L &= \pi\rho_\infty b^2\left[\dot{w} + U\cos\Lambda\dot{\theta} + U\sin\Lambda\dot{w}' - ab\ddot{\theta} - abU\sin\Lambda\dot{\theta}'\right] + C_{l\theta}\rho_\infty Ub\cos\Lambda \\
&\times[\dot{w}(0) + U\cos\Lambda\theta(0) + U\sin\Lambda w'(0) + \frac{b}{2}\left(\frac{C_{l\theta}}{\pi} - 1 - 2a\right)\dot{\theta}(0) \\
&+ \frac{b}{2}\left(\frac{C_{l\theta}}{\pi} - 1 - 2a\right)U\sin\Lambda\theta'(0)] + C_{l\theta}\rho_\infty Ub\cos\Lambda\int_0^t \phi(t-\sigma) \\
&\times[\dot{w} + U\cos\Lambda\dot{\theta} + U\sin\Lambda\dot{w}' + \frac{b}{2}\left(\frac{C_{l\theta}}{\pi} - 1 - 2a\right)\ddot{\theta} \\
&+ \frac{b}{2}\left(\frac{C_{l\theta}}{\pi} - 1 - 2a\right)U\sin\Lambda\dot{\theta}']d\sigma
\end{aligned} \tag{24}$$

$$\begin{aligned}
M &= \pi\rho_\infty b^3\left[\begin{array}{l} a\ddot{w} + U\sin\Lambda a\dot{w}' + U\cos\Lambda a\dot{\theta} - \frac{1}{2}\left(\frac{C_{l\theta}}{\pi} - 1\right)U\cos\Lambda\dot{\theta} - \frac{1}{2}\left(\frac{C_{l\theta}}{\pi} - 1\right) \\ \times U^2\sin\Lambda\cos\Lambda\theta' - b\left(\frac{1}{8} + a^2\right)\ddot{\theta} - b\left(\frac{1}{8} + a^2\right)U\sin\Lambda\dot{\theta}' \end{array}\right] \\
&+ C_{l\theta}\rho_\infty Ub^2\cos\Lambda\left(\frac{1}{2} + a\right)[\dot{w}(0) + U\cos\Lambda\theta(0) + U\sin\Lambda w'(0) + \frac{b}{2}\left(\frac{C_{l\theta}}{\pi} - 1 - 2a\right)\dot{\theta}(0) \\
&+ \frac{b}{2}\left(\frac{C_{l\theta}}{\pi} - 1 - 2a\right)U\sin\Lambda\theta'(0)] + C_{l\theta}\rho_\infty Ub^2\cos\Lambda\left(\frac{1}{2} + a\right)\int_0^t \phi(t-\sigma)[\dot{w} + U\cos\Lambda\dot{\theta} \\
&+ U\sin\Lambda\dot{w}' + \frac{b}{2}\left(\frac{C_{l\theta}}{\pi} - 1 - 2a\right)\ddot{\theta} + \frac{b}{2}\left(\frac{C_{l\theta}}{\pi} - 1 - 2a\right)U\sin\Lambda\dot{\theta}']d\sigma
\end{aligned} \tag{25}$$

In these equations, $\phi(t)$ is Wagner function.

4. Solution Methodology

Due to the intricacy of the aeroelastic governing equations, the solution is searched by using an approximate solution procedure. Also, to eliminate the time-dependent and parameter-dependent integral terms, some techniques are employed which discussed in this section.

4.1. *The parameter-dependent integral parts*

In order to eliminate the parameter-dependent integral parts, using a new class of generalized functions and by part integral method, the integral terms lead to partial-differential terms. A new class of generalized functions are derived from hyperbolic tangent family *tanh(nx)* as follows [50]:

$$\delta_{D,n}{}^{2} = \frac{n}{3}\delta_{D,n} - \frac{1}{12n}\delta''_{D,n} \tag{26}$$

$$\delta_{D,n}\delta''_{D,n} = -\frac{4n^3}{15}\delta_{D,n} + \frac{n}{6}\delta''_{D,n} - \frac{1}{40n}\delta^{(4)}{}_{D,n} \tag{27}$$

$$\delta_{D,n}{}^{3} = \frac{2n^2}{15}\delta_{D,n} - \frac{1}{24}\delta''_{D,n} + \frac{1}{480n^2}\delta^{(4)}{}_{D,n} \tag{28}$$

4.2. *The time-dependent integral parts*

In order to remove the time-dependent integral parts, using part integral method and some mathematical simplifications, Eqs. (16-19) convert into the equations which the time-dependent integral terms are eliminated as Refs. 24 and 25.

4.3. *The numerical approach*

Since an analytical solution for the equations of Appendix is difficult, the assumed modes method is employed herein. The bending and torsion deflections (w_f, θ_f, w_r, θ_r) are expanded by means of series of trial functions which only must satisfy geometric boundary conditions.[17]

$$w_{f,r}\left(x_{f,r},t\right) = \sum_{i=1}^{n} w_{f,r_i}\left(x_{f,r}\right)\cdot\eta_{f,r_i}\left(t\right) \tag{29}$$

$$\theta_{f,r}\left(x_{f,r},t\right) = \sum_{i=1}^{n} \varphi_{f,r_i}\left(x_{f,r}\right)\cdot\psi_{f,r_i}\left(t\right) \tag{30}$$

η_i and ψ_i are time-dependent functions of bending and torsional modes, respectively. Also w_i and ϕ_i indicate mode shapes for wing bending and torsional deflection, respectively, and can be expressed as Ref. 17:

$$w_{f,r_i}\left(x_{f,r},t\right)=\frac{\left(\frac{x_{f,r}}{l_{f,r}}\right)^{i+1}\left\{6+i^2\left(1-\frac{x_{f,r}}{l_{f,r}}\right)^2+i\left[5-6\frac{x_{f,r}}{l_{f,r}}+\left(\frac{x_{f,r}}{l_{f,r}}\right)^2\right]\right\}}{i\left(i+1\right)\left(i+2\right)\left(i+3\right)} \tag{31}$$

$$\varphi_{f,r_i}\left(x_{f,r}\right)=\sin\left(\frac{i\pi x_{f,r}}{l_{f,r}}\right) \tag{32}$$

By applying Eqs. (31, 32) into Eqs. (29, 30) and substituting them into the equations of Appendix, the following set of ordinary differential governing equations is obtained.

$$\left[\mathbf{M}\right]\left\{\ddot{\mathbf{q}}\right\}+\left[\mathbf{C}\right]\left\{\dot{\mathbf{q}}\right\}+\left[\mathbf{K}\right]\left\{\mathbf{q}\right\}+\left[\mathbf{H}\right]_t+\left[\mathbf{K}^0\right]_{I.Cs}\left\{\mathbf{q_0}\right\}=\left[\mathbf{0}\right] \tag{33}$$

where [**M**], [**C**] and [**K**] refer to the mass, damping and stiffness matrices, respectively and [**q**] denotes the generalized coordinate column vector. It is noteworthy that $[\mathbf{H}]_t$ and $[\mathbf{K^0}]_{I.Cs}$ matrices are related to the integral parts and initial conditions, respectively and have no effect on the flutter boundary. The final form of Eq. (33) in the state-space form is:

$$\left\{\dot{\mathbf{X}}\right\}=\left[\mathbf{A}\right]\left\{\mathbf{X}\right\} \tag{34}$$

[**q**] and {**X**} vectors are defined as

$$\left\{\mathbf{q}\right\}=\left\{\mathbf{q_1}^T\quad\mathbf{q_2}^T\right\}^T \tag{35}$$

$$\left\{\mathbf{X}\right\}=\left\{w_f\ \theta_f\ w_r\ \theta_r\ \dot{w}_f\ \dot{\theta}_f\ \dot{w}_r\ \dot{\theta}_r\ \ddot{w}_f\ \ddot{\theta}_f\ \ddot{w}_r\ \ddot{\theta}_r\ \dddot{w}_f\ \dddot{\theta}_f\ \dddot{w}_r\ \dddot{\theta}_r\right\}^T \tag{36}$$

For the determination of flutter, the problem is reduced to that of finding the eigenvalues of the matrix [**A**] for given values of the air speed parameter U_∞. The eigenvalue ω is a continuous function of the air speed U_∞. For $U_\infty \neq 0$, ω is in general a complex value, ω = Re (ω) + i Im (ω). When Re (ω) = 0 and Im (ω) ≠ 0 the wing is said to be in critical flutter condition and when Re (ω) = 0 and simultaneously Im (ω) = 0, the wing is said to be in critical divergence condition.

5. Numerical Results

In order to validate the solution procedure of the equations, a box wing configuration is considered as Ref. (15) and a schematic model is shown in Fig. 3.

A structural model of the box wing is implemented in MSC PATRAN as shown in Fig.4. The characteristics of the front and rear wings and also 1-D and 2-D elements are presented in Table 1 and 2, respectively.

The flutter analysis is performed by Doublet Lattice theory and PK method at the sea-level (ρ_∞=1.226 Kg/m^3). It should be noted that to determine the range of reduced

frequency, the maximum and minimum velocities and frequencies are indicated in Table 3.

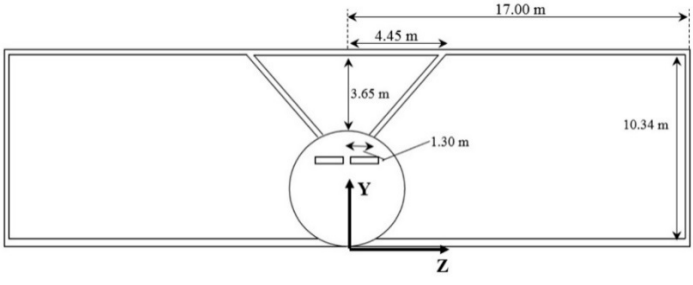

(a)

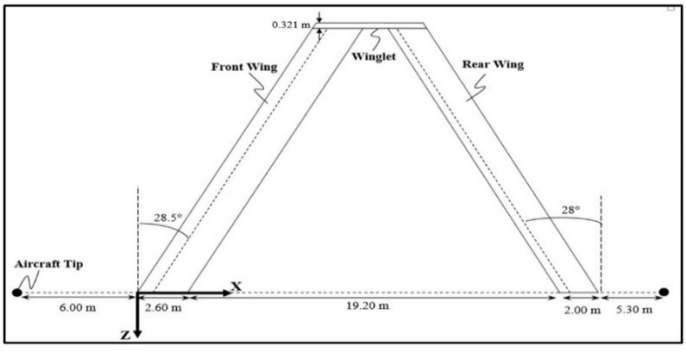

(b)

Fig. 3. (a) Front view (b) Top view of the BWA configuration

The specifications of the box wing are extracted by MSC NASTRAN and are presented in Table 4. Also, the following non-dimensional parameters are made: [48]

$$V_F = \frac{U_F}{b_f \omega_{\theta f}} \qquad K = \frac{k_s . l_s}{(EA)_s} \qquad B = \frac{b_f}{b_r}$$

$$\lambda = \frac{E_f . I_f}{E_r . I_r} \qquad \beta = \frac{G_f . J_f}{G_r . J_r} \qquad AR = \frac{l}{b} \tag{37}$$

where $(EA)_s$ and l_s are winglet tension stiffness and length, respectively and ω_θ is the first torsional frequency of the front wing.

A comparison between the approximate calculated mass of the box wing in MSC NASTRAN and Ref. (15) is demonstrated in Table 5. Also, the flutter analyses of the box wing are compared in Table 6. The results show a good agreement between numerical and software results for $K_s = 0.5$.

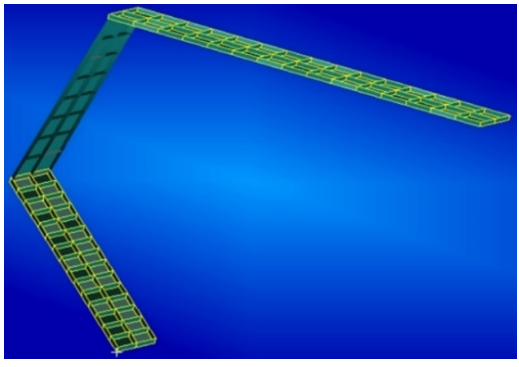

Fig. 4. The structural model of the box wing in MSC PATRAN

Table 1. The characteristics of the front and rear wings

Parameters	Unit	Value	Parameters	Unit	Value
b_f	m	1.3	b_r	m	1
l_f	m	19.344	l_r	m	19.254
Λ_f	°	28.5	Λ_r	°	-28
AR_f	-	13.077	AR_r	-	17
$(t/c)_f$	-	0.15	t/c_r	-	0.15
E_{Al}	N/m^2	7.0E+10	Span	m	34
E_{St}	N/m^2	2.0E+11	ρ_{Al}	Kg/m^3	2700
ν_{Al}	-	0.35	ρ_{St}	Kg/m^3	7800
ν_{St}	-	0.35	ρ_{air}	Kg/m^3	1.226

Table 2. The characteristics of 1-D and 2-D elements in MSC PATRAN

1D Elements	Number	Area, m^2	2D Elements	Number	Thick. (m)
Front Wing					
Post (St)	48	5.00E-05	Skin (Al)	60	0.021
Lead Spar Cap (St)	30	0.0005	Lead Spar (Al)	15	0.003
Center Spar Cap (St)	30	0.004	Center Spar (Al)	15	0.005
Trail Spar Cap (St)	30	0.0005	Trail Spar (Al)	15	0.003
Rib Cap (St)	64	5.00E-05	Rib (Al)	32	0.0005
Rear Wing					
Post (Al)	48	5.00E-05	Skin (Al)	60	0.02
Lead Spar Cap (Al)	30	0.0005	Lead Spar (Al)	15	0.003
Center Spar Cap (St)	30	0.004	Center Spar (Al)	15	0.005
Trail Spar Cap (Al)	30	0.0005	Trail Spar (Al)	15	0.003
Rib cap (Al)	64	5.00E-05	Rib (Al)	32	0.0005
Winglet					
Post	0	-	Skin (Al)	32	0.003
Lead Spar Cap	0	-	Lead Spar (Al)	8	0.01
Center Spar Cap	0	-	Center Spar (Al)	8	0.02
Trail Spar Cap	0	-	Trail Spar (Al)	8	0.01
Rib cap	0	-	Rib (Al)	9	0.02

Table 3. Determination of the range of reduced frequencies

Parameter	Value
Min. Frequency (Hz)	1
Max. Velocity (m/s)	350
Max. Frequency (Hz)	18
Min. Velocity (m/s)	140
Min. Boxes/Wavelength	14.8
Max. Box Aspect Ratio	3.01

Table 4. Characteristics of the box wing

Parameters	Unit	Value	Parameters	Unit	Value
EI_f	$N.m^2$	4.156E+08	EI_r	$N.m^2$	1.359E+08
GJ_f	$N.m^2$	7.760E+07	GJ_r	$N.m^2$	4.490E+07
m_f	Kg/m	349.92	m_r	Kg/m	268.62
$I_{\theta f}$	Kg.m	150.38	$I_{\theta r}$	Kg.m	63.68
b_f	m	1.3	b_r	m	1
a_f	-	0	a_r	-	0
$x_{\theta f}$	m	0	$x_{\theta r}$	m	0
l_f	m	19.344	l_r	m	19.254
Λ_f	°	28.5	Λ_r	°	-28
AR_f	-	13.077	AR_r	-	17
$l_{winlget}$	m	10.34	$EA_{winglet}$	N	1.865E+09

Table 5. Validation of the mass estimation for the box wing

Component, Mass (Kg)	Present	Ref. (15)	Error (%)
Front Wing	6769	6704	0.97
Rear Wing	5172	5009	3.25
Winglet	1026	1000	2.6
Total mass	12967	12713	2.0

The damping variation of the box wing in NASTRAN software, is plotted versus the airstream speed in Fig. 5.

Table 6. Validation of the flutter analysis for the box wing

Component	Computational Method	V_F (m/s)	ω_F (Hz)	Mach No.
Front Wing	Wagner Theory	287	4.58	0.84
	MSC NASTRAN	289	3.29	0.85
Rear Wing	Wagner Theory	274	6.89	0.81
	MSC NASTRAN	271	6.75	0.80
Box-Wing	Wagner Theory	269	6.55	0.79
	MSC NASTRAN	270	4.63	0.79

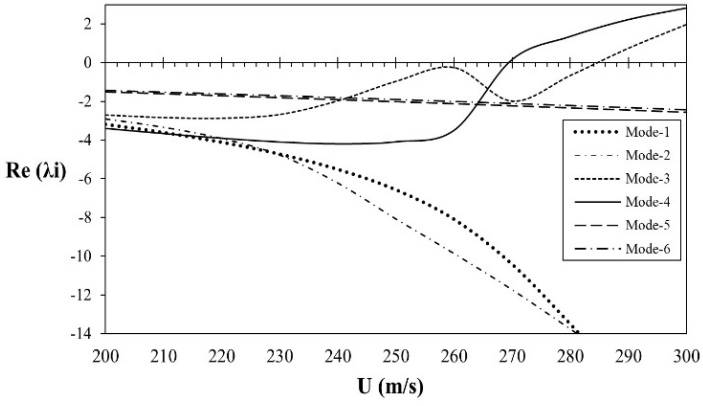

Fig. 5. The Damping variation vs. airstream speed for the box wing

Furthermore, in Fig. 6, in order to validate the Wagner aerodynamic model, the swept Goland wing is used. It can be observed that the accuracy of the flutter analysis is desirable and the numerical simulation has good agreement with the published papers.

It is worth noticing that $C_{l\theta}$ coefficient should be corrected as $C_{l\theta} = 2\pi\, AR/(AR\sqrt{1+(2cos\Lambda/AR)^2}+2cos\Lambda)$ for high sweep angles ($\Lambda > 30°$) and considered as $C_{l\theta} = 2\pi$ for sweep angles $\Lambda \leq 30°$. In Fig. 7, the effect of winglet tension stiffness on the flutter boundary is exhibited. As it can be observed in Fig. 7a, the stiffness has an optimum value for the flutter speed such that the maximum flutter speed is occurred at K=0.2. Fig. 7b shows that increasing the stiffness increases the flutter frequency, generally.

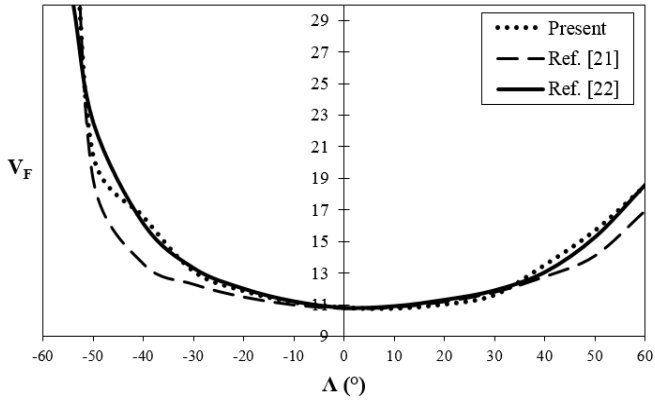

Fig. 6. Validation of the flutter speed for a swept Goland wing

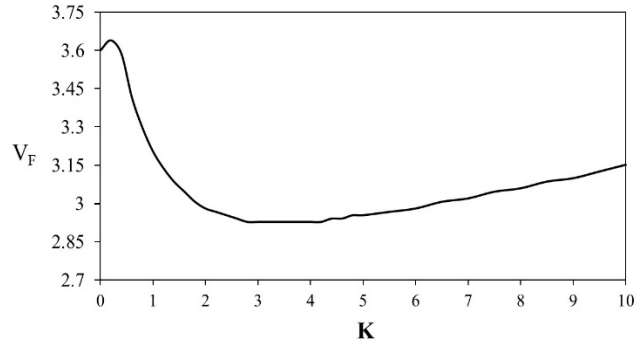

(a)

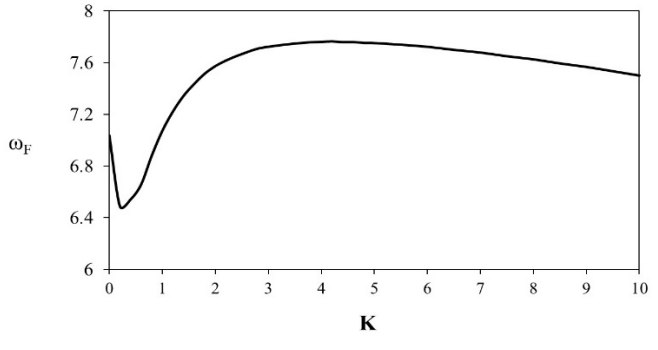

(b)

Fig. 7. Effects of the winglet tension stiffness on the flutter boundary (a) Flutter velocity (b) Flutter frequency

Fig. 8 demonstrates the effect of the front wing dihedral angle on the flutter velocity for selected values of winglet stiffness. It can be seen that the dihedral angle has no significant influence on the flutter boundary.

The effect of the box wing sweep angle on the flutter speed and frequency is presented in Fig. 9. The results show that increasing the sweep angle will expand the flutter stability boundary, especially for large sweep angles. But, by increasing the front and rear wings sweep angles, the flutter frequency does not change, significantly.

Figure 10 shows the effect of aircraft altitude on the flutter boundary for some selected sweep angles. It can be observed that the flutter speed increases at high altitudes and large sweep angles and the flutter frequency remains almost constant for large sweep angle. Also, effects of the front and rear wing sweep angles on the box wing flutter boundary is demonstrated in Fig. 11 for selected values of the chord ratios. The sweep angle has a minor influence on the flutter speed for the selected values of chord ratio as shown in Fig. 11a. However, increasing the chord ratio enhances the flutter speed and frequency.

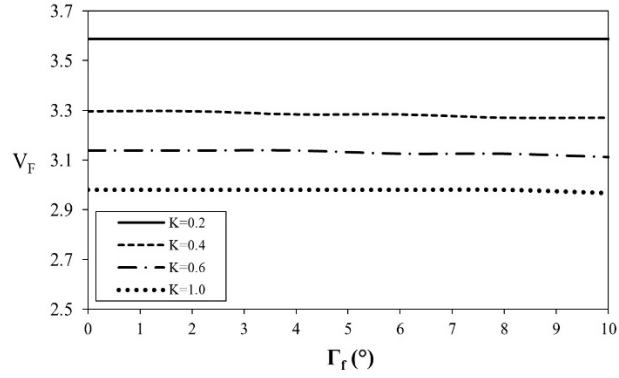

Fig. 8. Effects of the front wing dihedral angle on the flutter speed

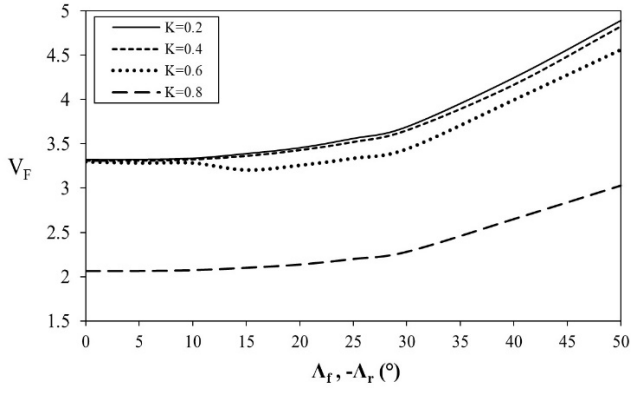

(a)

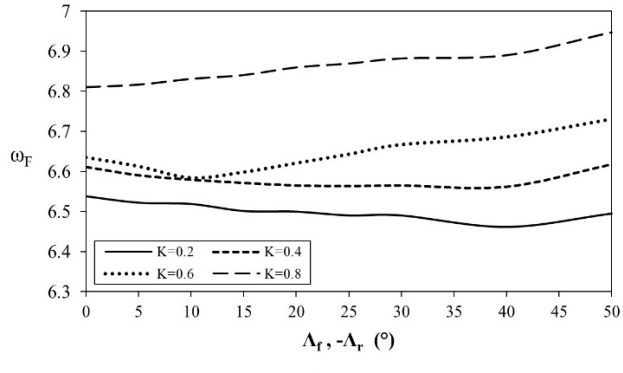

(b)

Fig. 9. Effects of the sweep angle on the flutter boundary (a) Flutter velocity (b) Flutter frequency

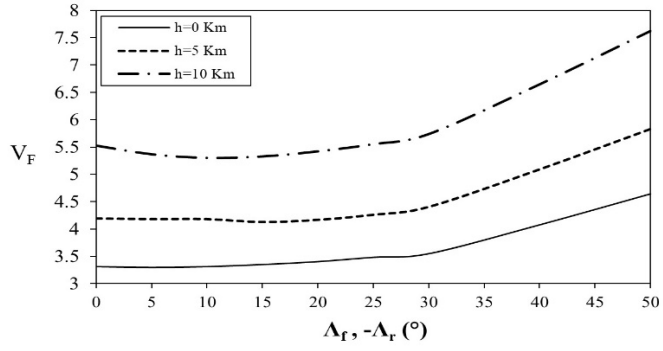

(a)

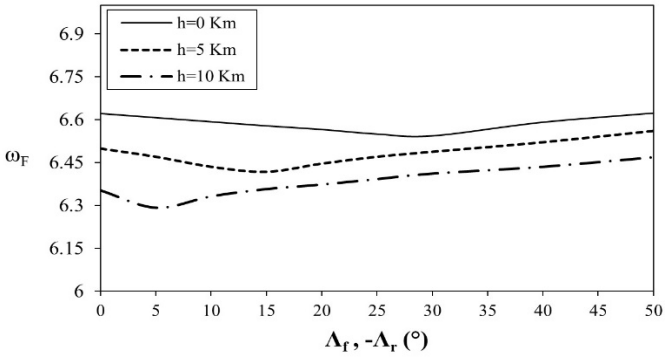

(b)

Fig. 10. Effects of the aircraft altitude on the flutter boundary (a) Flutter velocity (b) Flutter frequency

Figures 12 and 13 show the effects of bending and torsional rigidity ratio on the flutter boundary for selected values of the winglet stiffness, respectively. According to Fig. 12, increasing the bending rigidity ratio has no effect on the flutter speed at the high winglet stiffness but diminishes the flutter frequency. However, increasing the torsional rigidity ratio significantly decreases the flutter speed and frequency as shown in Fig. 13.

The final parameter that is investigated herein is the box wing span. Fig. 14a demonstrates that adding up the semi-span reduces the flutter speed dramatically at the first and then it remains constant; whereas the flutter frequency shows a completely decreasing trend as shown in Fig. 14b. On the other hand, increasing the winglet tension stiffness decreases the flutter speed and does not change the flutter frequency.

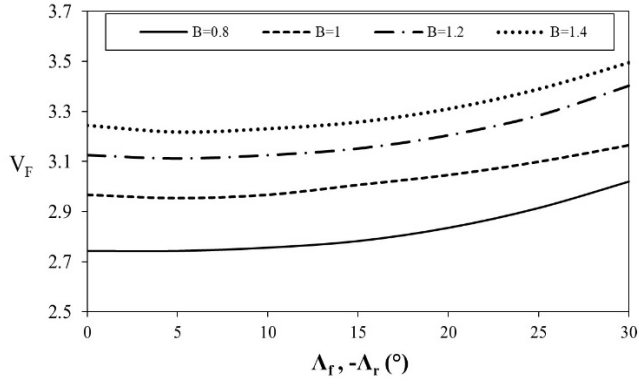

(a)

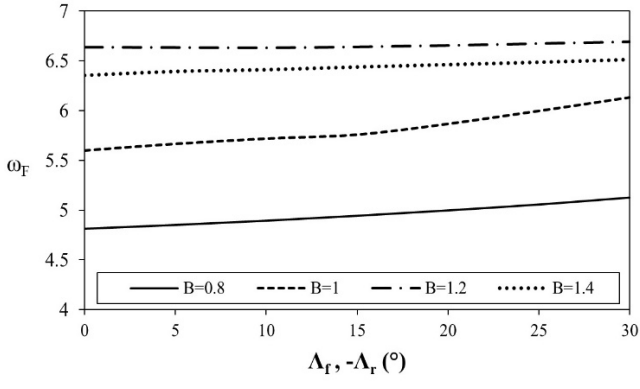

(b)

Fig. 11. Effects of the chord ratio on the flutter boundary (a) Flutter velocity (b) Flutter frequency

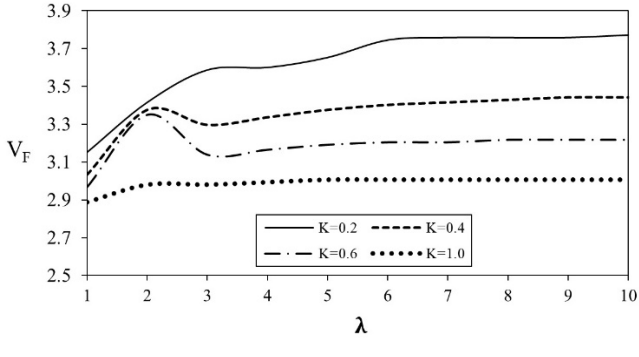

(a)

Fig. 12. Effects of the bending rigidity ratio on the flutter boundary (a) Flutter velocity (b) Flutter frequency

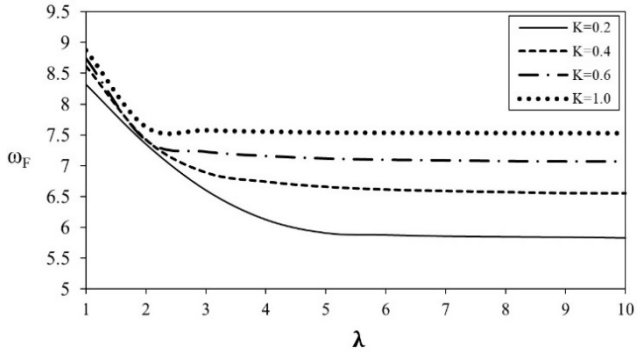

(b)

Fig. 12. (Continued)

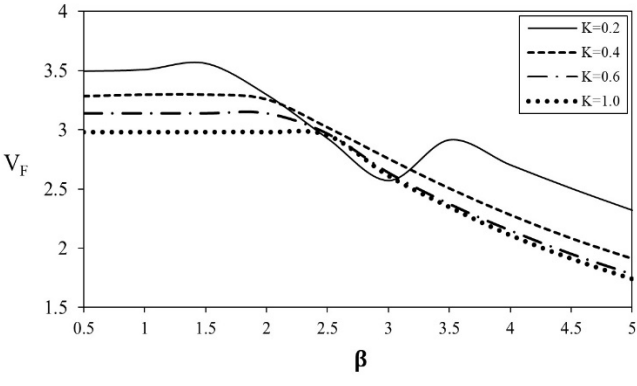

(a)

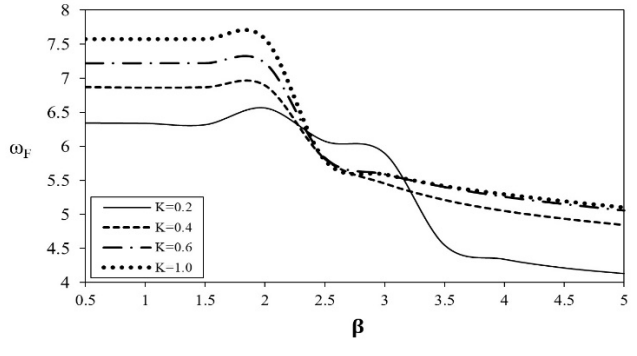

(b)

Fig. 13. Effects of the torsional rigidity ratio on the flutter boundary (a) Flutter velocity (b) Flutter frequency

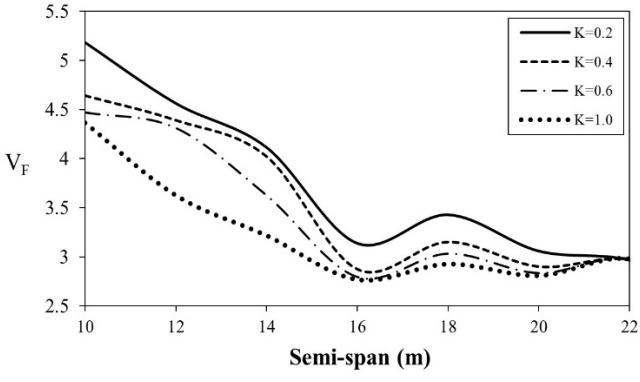

(a)

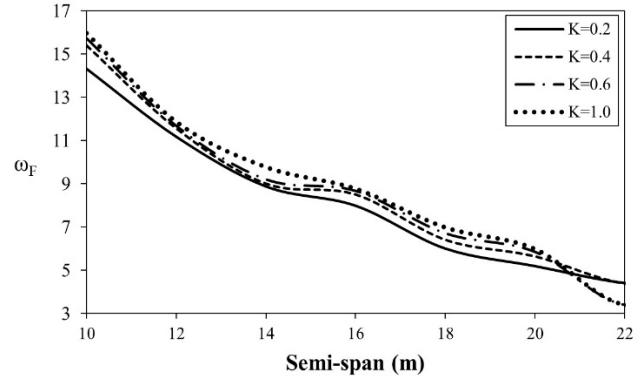

(b)

Fig. 14. Effects of the box wing span on the flutter boundary (a) Flutter velocity (b) Flutter frequency

6. Conclusions

In this paper, mathematical modeling of a 3-D box wing configuration is examined. The resulting aeroelastic partial integro-differential equations are solved by a multi-step procedure and the flutter results are validated with the results of MSC NASTRAN software and previous published papers. The Wagner unsteady model is used to apply the aerodynamic loadings to the equations and in order to analyze the model in MSC NASTRAN, PK method using Doublet-Lattice Subsonic Lifting Surface theory was utilized at the sea-level. Furthermore, the winglet is modeled by a longitudinal spring and the effect of the wing-joint interactions (bending and torsion coupling) is considered by placing two ends of the spring on the gravity centers of the front and rear wing tip sections.

The effects of some design parameters such as winglet tension stiffness, front and rear wings sweep and dihedral angles and aircraft altitude on the flutter boundary are studied.

The analyses revealed that winglet design has a significant influence on the box wing flutter boundary and the following consequences can be resulted:

- The maximum flutter speed of the box wing occurs at an optimum winglet stiffness (K=0.2) and on the other hand, a large increase in the winglet stiffness can diminish the flutter velocity.
- The dihedral angle of the front wing has no effect on the flutter boundary but the sweep angle of the box wing has a significant influence on the flutter speed, while it has a minor effect on the flutter frequency.
- While the chord ratio of the box wing increases, the flutter speed grows up, significantly.
- Increasing the box wing span reduces the flutter speed and frequency.

References

1. L. Prandtl, *Induced drag of multiplanes*, Technical Report TN182, NACA, Reproduction of Der induzierte Widerstand von Mehrdeckern, (1924) pp.309–315.
2. J. Wolkovitch, The joined wing aircraft: an overview, *J. Aircraft*. **23**(3) (1986) 161–178.
3. E. Livne and T.A. Weisshaar, Aeroelasticity of nonconventional airplane configurations: past and future, *J. Aircraft*. **40**(6) (2003) 1047–1065.
4. E. Livne, Aeroelasticity of joined-wing airplane configurations: past work and future challenges- a survey, *Proceeding of 42nd AIAA/ASME/ASCE/AHS/ASC Structures, Structural Dynamics, and Materials Conference*, Seattle, Washington (2001).
5. R. Cavallaro and L. Demasi, Challenges, ideas and innovations of joined-wing configurations: An aspect from the past, an opportunity for the future, *J. Progress in Aerospace Sciences*. **87** (2016) 1-93.
6. C. Bottani and J. Scanu, Preliminary design of a 250 passenger PrandtlPlane aircraft, Master of Science Thesis, University of Pisa, Italy (2004).
7. E. Torenbeek, and H. Deconinck, *Innovative configurations and advanced concepts for future civil aircraft* (Von Karman Institute for Fluid Dynamics, 2005).
8. A. Frediani, E. Rizzo, V. Cipolla, L. Chiavacci, C. Bottoni, J. Scanu and G. Iezzi, Development of ULM PrandtlPlane aircraft and flight tests on scaled models, *XIX AIDAA Congress*, Forlì, Italy (2007).
9. P. Jansen and R. Perez, Effect of size and mission requirements on the design optimization of non-planar aircraft configurations, *Proceeding of 13th AIAA/ISSMO Multidisciplinary Analysis Optimization Conference*, AIAA 2010-9188, Fort Worth, Texas (2010).
10. M. Barcala, C. Cuerno-Rejado, S. del Giudice, F. Gandía-Agüera and A.A. Rodríguez-Sevillano, Experimental investigation on box-wing configuration for UAS, *26th Bristol International Unmanned Air Vehicle Systems Conference*, Bristol, UK (2011).
11. A. Frediani, V. Cipolla and F. Oliviero, IDINTOS: the first prototype of an amphibious PrandtlPlane-shaped aircraft, J. Aerospace Science and Technology. **94**(3) (2015) 100–114.
12. G. Chiocchia, G. Iuso, E. Carrera and A. Frediani, A wind tunnel model of ULM configuration of PrandtlPlane: design, manufacturing and aerodynamic testing, *17th National Congress AIDAA*, XVII Congresso Nazionale AIDAA, Rome, Italy (2003).
13. C.C. Rasmussen, R.A. Canfield and M. Blair, Joined-wing sensor-craft configuration design, *J. Aircraft*. **43**(5) (2006) 1470–1478.
14. E. Rizzo, Optimization methods applied to the preliminary design of innovative-non conventional aircraft configurations, PhD Thesis, University of Pisa, Italy (2007).

15. D. Schiktanz, Conceptual design of a medium range box wing aircraft, Master of Science Thesis, Hamburg University of Applied Sciences, Germany (2011).
16. D. Scholz and R.C. Calleja, Design aspects of passenger box wing aircraft, *3rd Symposium on Collaboration in Aircraft Design*, Aircraft Design and Systems Group (AERO), Linkoping, Sweden (2013).
17. S.A. Fazelzadeh, A.H. Ghasemi, and A. Mazidi, Aeroelastic analysis of unrestrained aircraft wing with external stores under roll maneuver, *J. Acoustics and Vibration*. **21**(3) (2016) 327-333.
18. M. Goland and N.Y. Buffalo, The flutter of a uniform cantilever wing, *J. Applied Mechanics*. **12** (1945) 197-208.
19. D.H. Hodges and E.H. Dowell, *Nonlinear equations of motion for the elastic bending and torsion of twisted non-uniform rotor blades*, Report for NASA, Report no. TN D-7818 (1974).
20. S.A. Fazelzadeh, P. Marzocca, A. Mazidi and A.R. Rahmati, The effect of multiple stores arrangement on flutter speed of a shear deformable wing subjected to pull-up angular velocity, *Aeronautical J.* **113** (2009) 661-668.
21. A. Mazidi and S.A. Fazelzadeh, Flutter of a swept aircraft wing with a powered engine, *J. Aerospace Engineering*. **23** (2010) 243-250.
22. C. Karpouzian and L. Librescu, Non-classical effects on divergence and flutter of anisotropic swept aircraft wings, *J. AIAA*. **34** (1996) 786-794.
23. Z. Qin and L. Librescu, Aeroelastic instability of aircraft wings modeled as anisotropic composite thin-walled beams in incompressible flow, *J. Fluids and Structures*. **18** (2003) 43-61.
24. Sh. Shams, H. Haddadpour, M.H. Sadr Lahidjani and M. Kheiri, An analytical method in computational aeroelasticity based on Wagner function, *25th International Congress of the Aeronautical Sciences*, California, USA (2006).
25. Sh. Shams, M.H. Sadr Lahidjani and H. Haddadpour, Nonlinear aeroelastic response of slender wings based on Wagner function, *J. Thin-Walled Structures*, **46** (2008) 1192-1203.
26. R.H. Lange, J.F. Cahill, E.S. Bradley, R.R. Eudaily, C.M. Jenness and D.G. Macwilkinson, *Feasibility study of the transonic biplane concept for transport aircraft Applications*, NASA CR-132462, Lockheed-Georgia Company (1974).
27. E. Alyanak, and G. Brooks, Aeroelastic analysis of sensor-craft configurations using AVUS and NASTRAN, *Proceeding of 48th AIAA Aerospace Science Meeting Including the New Horizons Forum and Aerospace Exposition*, AIAA 2010-49, Orlando, Florida (2010).
28. P.S. Beran, N.S. Khot, F.E. Eastep, R.D. Snyder and J.V. Zweber, Numerical analysis of store-inducted limit-cycle oscillation, *J. Aircraft.* **41**(6) (2004) 1315-1326.
29. L. Di Palma, N. Paletta and M. Pecora, Aeroelastic design of a joined-wing UAV, *Aerospace Technology Conference and Exposition,* SAE Technical Paper 2009-01-3150 (2009).
30. M. Kurdi, N. Lindsley and Ph. Bern, Uncertainty quantification of the Goland wing's flutter boundary, *AIAA Atmospheric Flight Mechanics Conference and Exhibit*, South Carolina (2007).
31. P. Pereira, L. Almeida, A. Suleman, V. Bond, R. Canfield and M. Blair, Aeroelastic scaling and optimization of a joined-wing aircraft concept, *Proceeding of 48th AIAA/ ASME/ASCE/AHS/ASC Structures, Structural Dynamics, and Materials Conference*, AIAA 2007-1889, Honolulu, Hawaii (2007).
32. H.H. Lin, J. Jhou and R. Stearman, Influence of joint fixity on the aeroelastic characteristics of a joined-wing structure, *Proceeding of 31st AIAA/ASME/ASCE/AHS/ASC Structures, Structural Dynamics, and Material Conference*, AIAA Paper 90-0980, Long Beach, California (1990).
33. F. Zhi-Chao, L. Zi-Qiang and L. Ji-Nan, Preliminary study on flutter scaling of high-aspect ratio wings, *International J. of Modern Physics.* **34**(14) (2020).
34. M. Blair, R.A. Canfield and R.W. Roberts Jr., Joined-wing aeroelastic design with geometric nonlinearity, *J. Aircraft*. **42**(4) (2005) 832–848.
35. R. Cavallaro, Nonlinear aeroelastic analysis of joined-wing configurations, PhD Thesis, University of California, San Diego, USA (2014).

36. A. Alizadeh, Z. Ebrahimi, A. Mazidi and S.A. Fazelzadeh, Experimental Nonlinear Flutter Analysis of a Cantilever Wing/Store, *International J. Structural Stability and Dynamics*. **20**(7) (**2020**).
37. A.S. Mirabbashi, A. Mazdid and M.M. Jalili, Analytical and experimental flutter analysis of a typical wing section carrying a flexibly mounted unbalanced engine, *International J. Structural Stability and Dynamics*. **19**(2) (**2019**).
38. R.M. Ajaj, F.K. Omar, T.T. Darabseh and J. Cooper, Flutter of telescopic morphing wing, *International J. Structural Stability and Dynamics*. **19**(6) (**2019**).
39. M.H. Durham and R. Ricketts, Flutter of a joined-wing high altitude vehicle, Aerospace Flutter and Dynamic Council Meeting, October 19-20, Orlando, Florida, USA (1989).
40. J.M. Van Aken, *Alleviation of whirl-flutter on a joined-wing tilt-rotor aircraft configuration using active controls*, NASA CR-196103, NTIS N94-36436 (1991).
41. D.H. Lee, Aeroelastic tailoring and structural optimization of joined-wing configurations, PhD Thesis, Purdue University, USA (2002).
42. D.D. Canto, N. Divoux, A. Frediani, G.L. Ghiringhelli and M. Terraneo, Preliminary design against flutter of a PrandtlPlane lifting system, XX Congresso Nazionale AIDAA, Milan, Italy (2009).
43. N. Divoux and A. Frediani, The lifting system of a PrandtlPlane, Part 2: Preliminary study on flutter characteristics, *J. Variational Analysis and Aerospace Engineering*, **66** (2012) 235-267.
44. R. Bombardieri, PrandtlPlane joined-wing: body freedom flutter, limit cycle oscillation and freeplay studies, Master of Science Thesis, Pisa University, Italy (2015).
45. R. Bombardieri, R. Cavallaro and L. Demasi, A historical perspective on the aeroelasticity of box wings and PrandtlPlane with new findings, *Proceeding of 57th AIAA/ ASCE/AHS/ASC Structures, Structural Dynamics, and Materials Conference*, AIAA 2016-0238, San Diego, California (2016).
46. R. Cavallaro, R. Bombardieri, S. Silvani, L. Demasi and G. Bernardini, Aeroelasticity of the PrandtlPlane: body freedom flutter, freeplay and limit cycle oscillation (International Variational Analysis and Aerospace Engineering: Mathematical Challenges for Aerospace Design, Springer, Cham, 2016).
47. S. Silvani, Aeroelastic analysis of Prandtl Plane joined wings configuration, Master of Science Thesis, Universit'a degli Studi di Roma, Italy (2015).
48. S.A. Fazelzadeh, D. Scholz, A. Mazidi and M.I. Friswell, Flutter characteristics of typical wing sections of a box wing aircraft configuration, *Advanced Aircraft Efficient Global Air Transport System Conference*, AEGATS2018-003, Toulouse, France (2018).
49. PARSIFAL Project, *Aeroelastic analysis of the baseline PrandtlPlane*, Deliverable 5.2, Prandtlplane Architecture for the Sustainable Improvement of Future AirpLanes (2020).
50. R.C. Costen, *Products of some generalized functions*, Report for NASA, Report no. TN D-4244 (1967).

Preprint of an article published in International Journal of Structural Stability and Dynamics, vol. 22, no. 02, pp. 2250016-1 – 2250016-24. https://doi.org/10.1142/S021945542250016X.